Polylactic Acid/Cerium Fluoride Films: Effects of Cerium Fluoride on Mechanical Properties, Crystallinity, Thermal Behavior, and Transparency

Yincai Wu [1,2], Xintu Lin [1], Jinlei Li [2], Chuanxiang Zhang [1], Yuejun Liu [1,*], Lijun Song [2,3,*], Xihai Hao [1,*], Fenglong Lin [1,2], Shenglong Wang [2] and Tungalag Dong [4]

1   Key Laboratory of Advanced Packaging Materials and Technology of Hunan Province, School of Packaging and Materials Engineering, Hunan University of Technology, Zhuzhou 412007, China; xmwuyincai@fjirsm.ac.cn (Y.W.); xinxlin@126.com (X.L.); cxzhang7335@126.com (C.Z.); linlong9386@163.com (F.L.)
2   Xiamen Key Laboratory of Rare Earth Photoelectric Functional Materials, Xiamen Institute of Rare Earth Materials, Chinese Academy of Sciences, Xiamen 361021, China; 13997894639@163.com (J.L.); xmwangshenglong@fjirsm.ac.cn (S.W.)
3   Key Laboratory of Design and Assembly of Functional Nanostructures, Fujian Provincial Key Laboratory of Nanomaterials, Fujian Institute of Research on the Structure of Matter, Chinese Academy of Sciences, Fuzhou 350002, China
4   School of College of Food Science and Engineering, Inner Mongolia Agricultural University, Hohhot 010000, China; dongtlg@imau.edu.cn
*   Correspondence: yjliu_2005@126.com (Y.L.); slj@fjirsm.ac.cn (L.S.); 10583@hut.edu.cn (X.H.)

Abstract: PLA is widely used in the field of disposable products for its good transparency, high strength, high modulus, and good processing performance. However, the crystallization rate and crystallinity of PLA are weak. In actual production, the PLA products that are typically obtained are amorphous with poor heat resistance, which greatly limits the application range of PLA products. Finding an effective nucleating agent to improve the transparency of PLA has been a hot topic in research. This study found that Cerium fluoride (CeF_3) can effectively improve the crystallinity of PLA/CeF_3 (P/F) films. When the content of CeF_3 in PLA was 1 wt %, the retention ratio of visible light transmittance was 82.36%, the crystallinity was 29.8%, and the tensile strength was 59.92 MPa. Compared to pure PLA, the crystallinity of P/F1 increased by 56% and tensile strength increased by 8.76%. This study provided an alternative scheme that maintained the PLA film's transparency and improved the crystallinity of PLA, which significantly expanded the application of PLA.

Keywords: PLA; CeF_3; crystallinity; visible light transmittance; transparency

1. Introduction

Polylactic acid (PLA) is a kind of aliphatic thermoplastic polyester and biodegradable biobased polymer [1–10]. In contrast to traditional fossil-based polymers, it is one of the most promising biobased polymers that plays an important role in the polymer market [11–16]. It can effectively prevent and alleviate environmental problems such as "white pollution" [1–4,17]. Moreover, PLA is one of the most suitable candidate materials to replace polystyrene (PS), polyethylene terephthalate (PET), polyethylene (PE) and polypropylene (PP) [18–23]. Due to its good transparency, high strength, high modulus, and good processing performance, PLA has broad applications in the field of disposable products, such as food packaging, tableware, water cup, water bottle, etc.

However, the practical applications of PLA are limited because of its brittleness, poor toughness, low crystallinity, and fast crystallization speed [24,25]. Some physical properties, such as the mechanical, heat resistance and barrier properties of PLA, are correlated to its crystallinity [26]. So far, many studies have been conducted on the crystallization

behavior of PLA [27–30]. Generally, the crystallinity will be improved by chemical and physical methods. Chemical methods usually refer to manipulation of the PLA polymer structure at the molecular level, while physical methods are performed by expanding the nucleating agent to the crystalline region in the polymer matrix [31,32]. At present, there are two kinds of nucleating agents: organic nucleating agents and inorganic nucleating agents. Organic nucleators mainly include hydrazide, aliphatic amide, amide, etc., such as ethylenebisearamide [33], 1,2-hydroxystearamide [34], tmc-328 [35–37] and N,N'-bis(benzoyl) Diacylhydrazine hexanedioate [38], algal residue nanocellulose, etc. [39]. Inorganic nucleators mainly include montmorillonite, talc powder, mica, calcium carbonate, carbon nanotubes, graphene, magnesium oxide, etc. [40–45]. In some previous reports, adding a nucleating agent to PLA can not only increase crystallinity, but also improve its mechanical properties and thermal stability [44,45].

Due to their large ionic radius and unique electronic structure, rare earth elements exhibit high coordination number and strong coordination ability, especially with strong acid elements such as oxygen and sulfur [46]. In this paper, CeF_3 as the second phase was added to polylactic acid by means of coordinated interactions; cerium ions will play a special role in tuning the crystallinity and modifying the physical properties of PLA.

2. Materials and Methods

2.1. Materials

Poly(lactic acid) (PLA) (PLA, 3001D; MFR, 22 g/10 min; specific gravity, 1.24; melting point, 173 °C; crystallinity, 19%; optical purity, ≥96%; clarity, transparent) was obtained from Nature Works in pellet form. CeF_3 (boiling point, 2300 °C; melting point, 1640 °C; molecular weight, 197.1112; purity, 99.9%; specific density, 0.162; granularity, D50 = 1.16 μm) was obtained from the Hunan Institute of Rare Earth Materials.

2.2. Preparation of PLA/CeF₃ (P/F) Blends and Films

PLA and CeF_3 were dried at 70 °C for 4 h in a vacuum oven before further processing. PLA/CeF_3 (P/F) blends were prepared by using a torque rheometer (RT01-06/02, Guangzhou, China) in mass ratios of 100/0, 99.5/0.5, 99/1, 98/2, 97/3, and 96/4; the formulation of P/F mixtures is shown in Table 1. The rotating speed was 60 rpm at 180 °C for 5 min. Then, all the samples were hot-pressed onto 0.1 mm-thick sheets at 180 °C with a pressure of 15 MPa of 2 min, and then, cooled down to room temperature; samples were cold-pressed again, and the final P/F films were obtained. A schematic illustration of the preparation of P/F films is shown in Figure 1.
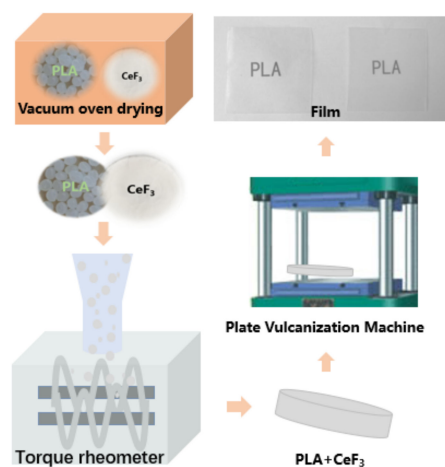
Figure 1. Schematic illustration of the preparation of P/F films.

Table 1. Formulation of P/F films by mass fraction percentage.

Samples	PLA	CeF$_3$
P/F0	100	0
P/F0.5	99.5	0.5
P/F1	99	1
P/F2	98	2
P/F3	97	3
P/F4	96	4

2.3. Characterizations

The tensile properties of the P/F films were tested by a universal material testing machine (Instron 2365, Darmstadt, Germany) at a crosshead speed of 50 mm/min according to the ASTM D638-2008 standard. The P/F films were conditioned at room temperature in a 50% relative humidity-controlled environment for at least 24 h prior to being tested. At least five runs for each sample were measured, and the results were averaged. Then, the tensile strength, Young's modulus and elongation at break of the samples were obtained. A Fourier transform infrared spectrophotometer (Nicolet iS 50, Madison, WI, USA) was used to investigate the possible intermolecular interaction between PLA and CeF$_3$. The average value was obtained from 32 scans in the standard wave-number range of 500 to 4000 cm^{-1}. A UV-visible-near infrared light spectrophotometer (Cary 5000, Santa Clara, CA, USA) was used to characterize the transmittance of the P/F films in the visible light region. The test wavelength range is 200–800 nm. Field emission scanning electron microscopy (FESEM) (Apreo S, Waltham, MA, USA) was used to characterize the cross-section and surface phase morphology of the P/F films. A layer of platinum was sputter-coated uniformly over all the fractured surfaces before FESEM observation. X-ray diffraction (Miniflex 600, Akishima-shi, Japan) was used to characterize the crystallinity of the P/F films. Measurements were performed over the ranges 5–70 °C, with a step of 0.05 °C and speed 10 °C/min. The thermal and crystallization behaviors of the PLA/CeF$_3$ blends were studied by differential scanning calorimetry (TGA/DSC 1, Zurich, Switzerland) under nitrogen atmosphere. The weight of the samples varied from 5.0 to 10.0 mg. The samples were heated from 30 °C up to 190 °C at 10 °C/min (the first heat scan) and held at 190 °C for 3 min to eliminate their previous thermal history. Following this, the samples were chilled to 30 °C at the same rate, and then, heated again from 30 °C up to 190 °C at 10 °C/min (the second heating scan). The thermal stability of the P/F films was studied by thermogravimetric analyses. Samples of about 5 mg were placed in alumina crucibles and were measured in dynamic conditions, in the temperature range from 30 to 600 °C, with a heating rate of 10 °C/min, and a 50 mL/min Ar$_2$ flow. Dynamic mechanical analysis was performed in a DMA instrument (DMA 1, Mettler Toledo, Zurich, Switzerland) in the tensile mode, based on the ASTM standard D4092. All samples were cut from the tensile bar specimens (40 mm × 10 mm × 0.1 mm). The temperature ranged from −20 to 100 °C, with a heating rate of 3 °C/min at an oscillating frequency of 1 Hz.

3. Results and Discussion

3.1. Mechanical Properties

As shown in Figure 2a, with the increase in CeF$_3$ content, the tensile strength and elongation at break of the P/F films increased at first and then decreased. When the content of CeF$_3$ was 1 wt %, the tensile strength of the P/F1 film was the highest, reaching from 55.09 to 59.92 MPa, which was 8.76% higher than that of pure PLA. When the content of CeF$_3$ was 2 wt %, the elongation at break of the P/F2 film was the highest, reaching 2.53%, which was 78% higher than that of pure PLA. The tensile stress–strain curves of P/F films are shown in Figure 2b. When the content of CeF$_3$ was 2 wt %, the overall effect of strengthening and toughening was better. This showed that CeF$_3$ improved the ductibility ability of P/F film in the range of 0.5% to 2%.
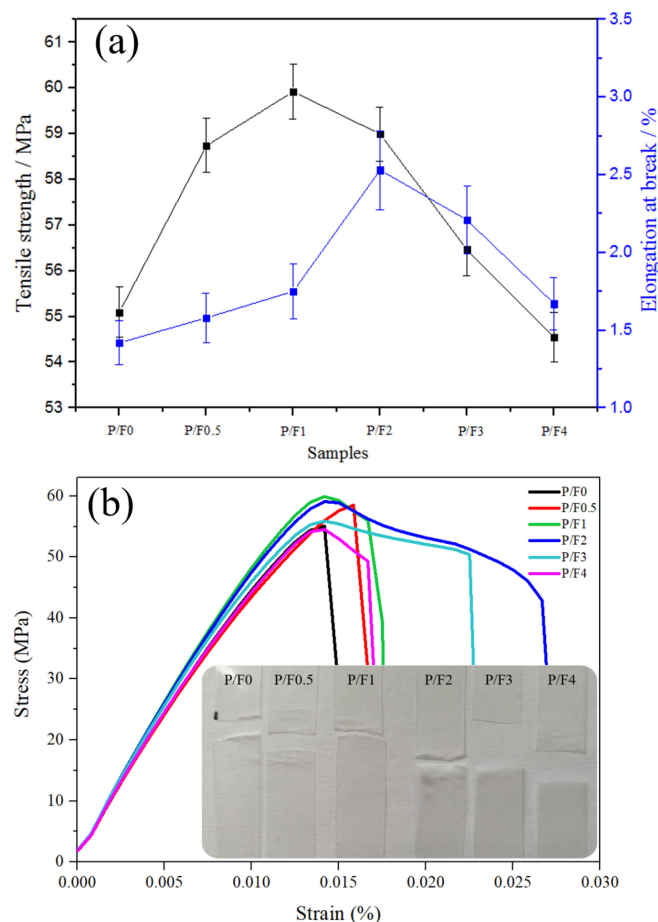
Figure 2. (**a**) Mechanical properties and (**b**) tensile stress–strain curves of P/F films.

3.2. Fourier Transform Infrared Spectrophotometer (FTIR)

The characteristic absorption peak of PLA included: $-CH_3$ asymmetric stretching vibration peaks observed at 3000 and 1460 cm^{-1}; symmetrical stretching vibration peaks were observed at 1380 cm^{-1}. The stretching vibration peak of $-C=O$ was observed at 1750 cm^{-1}. $-CH$ stretching and bending vibration peaks were observed at 2950 and 1360 cm^{-1}, respectively. The stretching vibration peaks of $-C-O-C-$ were 1260, 1180 and 1080 cm^{-1} [47–49].

As shown in Figure 3, compared with pure PLA (P/F0), the spectral peak of P/F4 had several new characteristic peaks in the range of 500~700 cm^{-1}. For example, these characteristic peaks (532, 543, 571, 578 and 598 cm^{-1}) of P/F4 represent the coordination interactions that exist between cerium and oxygen atoms in PLA. In addition, new characteristic peaks also appeared in 673 and 693 cm^{-1}. These two peaks were assigned to the vibration modes from the Ce-O band.

In general, the main characteristic peaks of PLA were retained, which proved that CeF$_3$ does not change the main structure of PLA, but had a certain coordination effect and coupling relationship. The coordination effect and coupling relationship were conducive to enhancing the mechanical properties of PLA, which was also verified by the mechanical property test results in Figure 2.
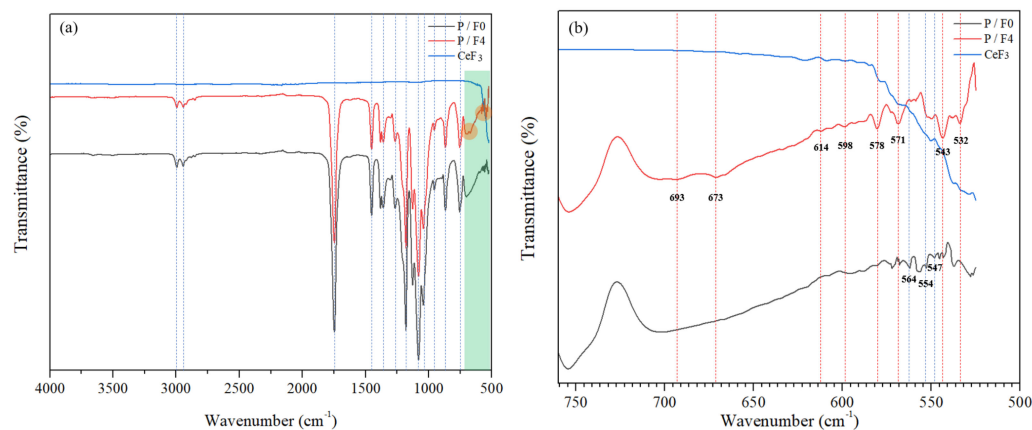
Figure 3. Infrared spectra of CeF_3, P/F0 and P/F4 films. (**a**) Wavenumber range 500–4000 cm^{-1}; (**b**) Wavenumber range 500–730 cm^{-1}.

3.3. UV–Vis Transmittance

In order to study the effect of CeF_3 on the visible light transmittance of P/F films, the UV–vis spectral transmittance of P/F films was measured. The calculation formula of visible light transmittance is the following relationship (Equation (1)):

$$T_v \% = \frac{T_{w760} \% + T_{w390} \%}{2} \tag{1}$$

where $T_v \%$ is the average visible light transmittance, $T_{w760} \%$ is the visible light transmittance at 760 nm, and $T_{w390} \%$ is the visible light transmittance at 390 nm.

Figure 4 shows that the visible light transmittance of P/F films decreased slightly with the increase in the addition of CeF_3 and the specific data, as shown in Table 2.
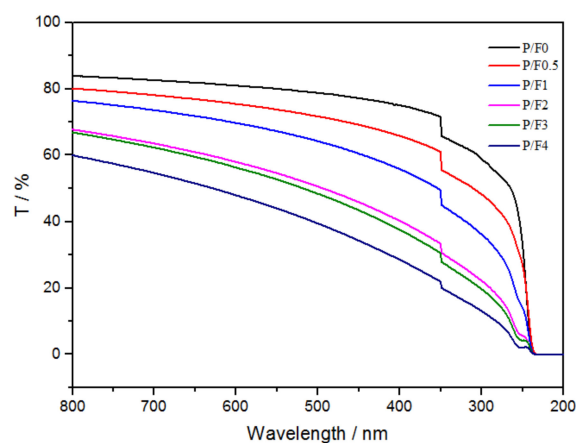
Figure 4. UV-vis transmittance of P/F films.

Table 2. Transmittance of P/F films in visible light with different amount of CeF_3.

Sample	Visible Light Transmittance/%
P/F0	78.97
P/F0.5	72.19
P/F1	65.04
P/F2	52.58
P/F3	50.71
P/F4	42.62

When the content of CeF$_3$ in PLA was 1 wt %, the visible light transmittance retention ratio of the P/F1 film was 82.36%. Pure PLA film and P/F1 film samples are shown in Figure 5.
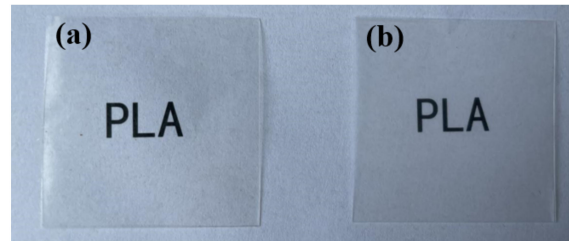
Figure 5. Pure PLA film (**a**) and P/F1 film (**b**) samples.

3.4. Morphological Properties

Figure 6 shows the cross-section and surface morphology of P/F films. The FESEM images show that CeF$_3$ were well dispersed in the P/F films, and there were few cavities in the brittle cross-section, which indicated that the interface between CeF$_3$ and PLA was good. This may be due to the formation of various coordination modes between cerium and oxygen in the hydroxyl and carboxyl groups of PLA, and the formation of layered, network polymers or infinite chain structure, which improved the compatibility of different components. It also indicated that the addition of CeF$_3$ could tune the strength and toughness of PLA, which was consistent with the test results of mechanical properties.
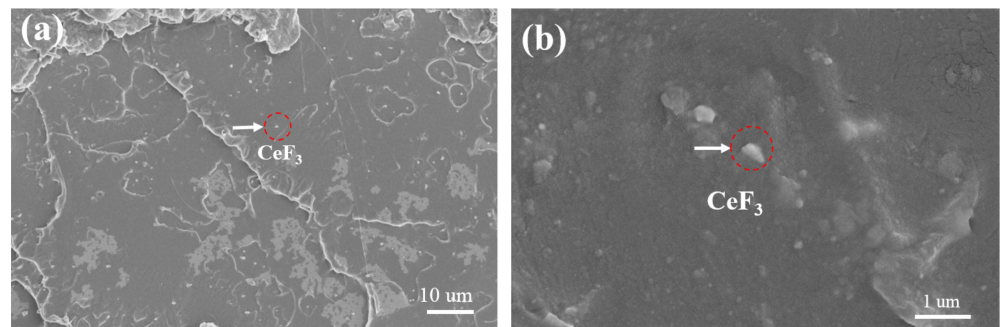
Figure 6. (**a**) Cross-section and (**b**) surface morphology of P/F2 films.

3.5. X-ray Diffraction (XRD)

In order to analyze the effect of CeF$_3$ on the crystal structure of PLA, the annealed P/F films were analyzed by XRD. Figure 7 shows the XRD patterns of P/F films annealed for 2 h at 110 °C. There was a diffuse hump peak of P/F0 without annealing between 5 and 25 °C, indicating that the P/F0 was in the amorphous state. When P/F0 was annealed for 2 h, only a weak crystallization peak appeared. However, when PLA was added to CeF$_3$, an obvious crystallization peak appeared. With the increase in CeF$_3$ content, the crystallization peak intensity increased first and then decreased slightly, which proved that a certain amount of CeF$_3$ was helpful to promote the crystallization of PLA.
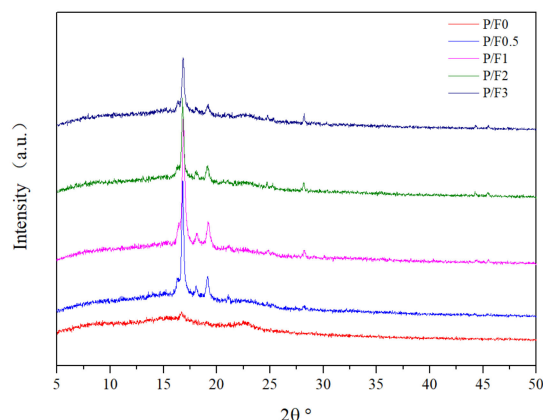
Figure 7. XRD patterns of P/F films annealed for 2 h at 110 °C.

3.6. Differential Scanning Calorimetry (DSC)

DSC analysis was carried out to investigate the melting and crystallization behaviors of the P/F films. The DSC second heating curves of P/F films are shown in Figure 8, which displayed three main transitions successively: a glass transition, a cold crystallization exotherm, and a melting endotherm. The measured values of the phase transition parameters are summarized in Table 3. With the increase in CeF_3 content, the glass transition temperature (T_g) of PLA hardly changed, suggesting that CeF_3 did not change the glass transition temperature of PLA. However, the addition of CeF_3 significantly decreased the cold crystallization temperature (T_{cc}) of PLA. When the CeF_3 content increased from 0.5 wt % to 4 wt %, the T_{cc} of P/F films decreased from 116.25 to 103.99 °C gradually and the ΔH_c gradually decreased from 10.97 to 1.87 J/g, indicating the addition of CeF_3 could accelerate the crystallization of PLA. The degree of crystallization of the sample was evaluated from the heat evolved during crystallization by the following relationship (Equation (2)):

$$X_c \% = \frac{\Delta H_m - \Delta H_c}{W_{PLA} \times \Delta H_m^0} \times 100 \% \tag{2}$$

where $X_c \%$ is the degree of crystallinity of the samples, ΔH_m is the heat of fusion of the PLA in the blend, ΔH_c is the enthalpy of cold crystallization of the PLA in the blend, $\Delta H_m^0 \Delta$ is the heat of fusion for 100% crystalline PLA (93.1 J/g) [34], and W_{PLA} is the weight fraction of PLA in the blend.
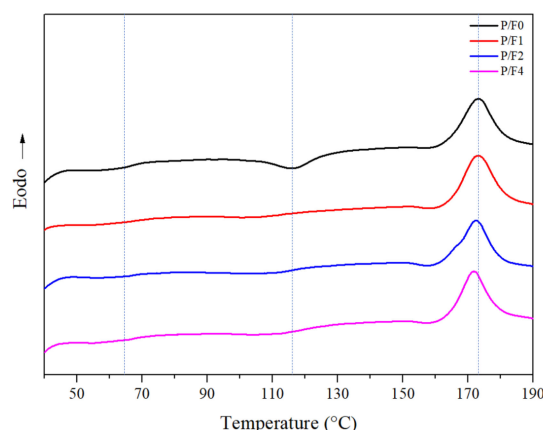
Figure 8. DSC second heating curves of P/F films.

Table 3. The phase transition parameters of P/F films.

Sample	T_{cc} (°C)	ΔH_c (J/g)	T_m (°C)	ΔH_c (J/g)	X_c (%)
P/F0	116.25	10.97	172.92	28.70	19.0
P/F1	103.99	1.87	173.21	29.62	29.8
P/F2	109.44	4.25	172.16	26.92	27.2
P/F4	109.21	1.41	171.79	26.19	26.6

When the content of CeF_3 in PLA was 1 wt %, the crystallinity was 29.8%, which was 56% higher than that of pure PLA. Other P/F films' crystallinity is shown in Table 3. The crystallization ability increased likely because of the coordination interaction between PLA and CeF_3 or heterogeneous nucleation in PLA, which might result in the ordered segmental arrangement of PLA chains. A schematic diagram of the interaction between CeF_3 and PLA is shown in Figure 9.
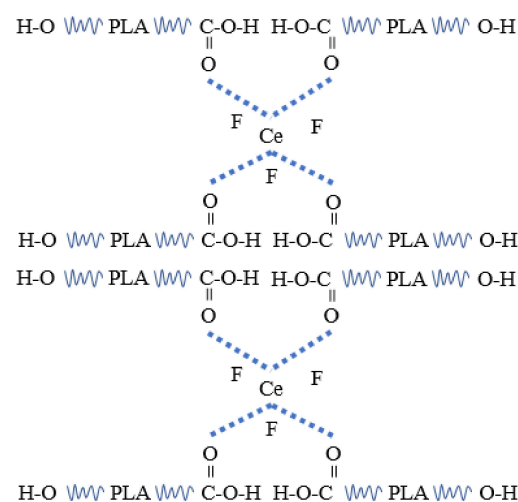
Figure 9. Schematic diagram of the interaction between CeF_3 and PLA.

3.7. Thermogravimetric Analyses (TGA)

The thermal stability of PLA is critical, as this property is considered as the limiting factor for processing as well as for end-use applications [50]. Figure 10 shows the TGA thermograms of the P/F films, and Table 4 presents a summary of thermal performance, i.e., the initial, 5% mass loss, maximum mass loss and final residue at 500 °C. The mass was barely lost before 100 °C, proving that the moisture in PLA was removed by drying before further processing. The TGA curve was a flat period before 250 °C, then dropped at 280–380 °C suddenly, and then, tended to be stable. It was a typical one-step degradation reaction [51]. After 500 °C, P/F almost decomposed completely.

Table 4. TGA data of P/F films.

Samples	$T_{5\%}$ Weight Loss (°C)	T_{max} Weight Loss (°C)	Reside at 500 °C (%)
P/F0	315.7	354.1	0.54
P/F1	318.5	357.6	1.53
P/F2	330.8	364.2	2.17
P/F4	308.4	355.7	4.52
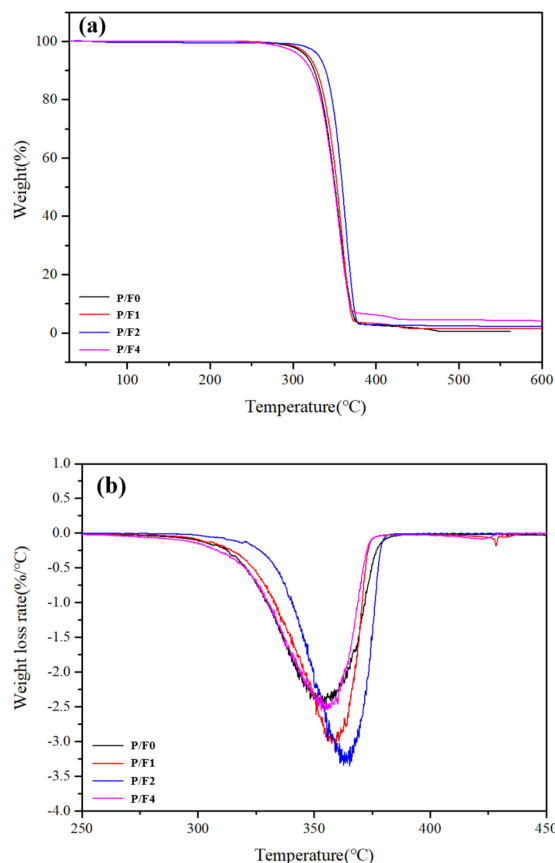
Figure 10. TGA (**a**) and DTG (**b**) of P/F films.

The initial thermal stability of the P/F film was like that of pure PLA. The TGA data of the P/F films are shown in Table 4. When the amount of CeF_3 was 2 wt %, the initial degradation temperature of P/F2 films was 330.8 °C, and the maximum degradation temperature was 364.2 °C, which was 15.1 and 10.1 °C higher than that of pure PLA, respectively. When the amount of CeF_3 was more than 2%, the initial decomposition temperature of the P/F1 film was lower than that of pure PLA, but the maximum degradation temperature was still higher than that of pure PLA. This was likely due to the effect of CeF_3 on the interaction between PLA chains. When at a lower temperature, the movement ability of PLA molecular chains was limited and the effect of CeF_3 on the interaction between PLA molecular chains was dominant. With the temperature increase, the movement ability of PLA molecular chains intensified, and the heterogeneous CeF_3 particles promoted the crystallization of PLA. Consequently, the DSC test results were confirmed, resulting in the improvement of the maximum degradation temperature of PLA. In general, CeF_3 was beneficial to improving the thermal stability of PLA.

3.8. Dynamic Mechanical Analysis (DMA)

DMA was used to analyze the miscibility and modulus changes of the P/F films. Figure 11a,b show the dependence of loss factor (tan δ) on the temperature for PLA mixtures with different contents of CeF_3. Only one tan δ peak was observed for P/F films, while pure PLA had a T_g of 65 °C. Figure 11a,b show that the incorporation of CeF_3 resulted in a small change in the glass transition temperature of PLA. The tan δ peaks of all the P/F films (near 65 °C) were between that of pure PLA. As shown in Figure 11b, the storage modulus (E′) of pure P/F films gradually decreased with the increasing CeF_3 component, and the storage modulus (E′) of the P/F2 films was 1000 MPa, which was 63.6% lower than that of pure PLA. This suggested that P/F films showed a lower storage modulus than pure PLA from −20 to 60 °C, which showed that CeF_3 had increased the flexibility of PLA, which was consistent with the test results of mechanical properties.
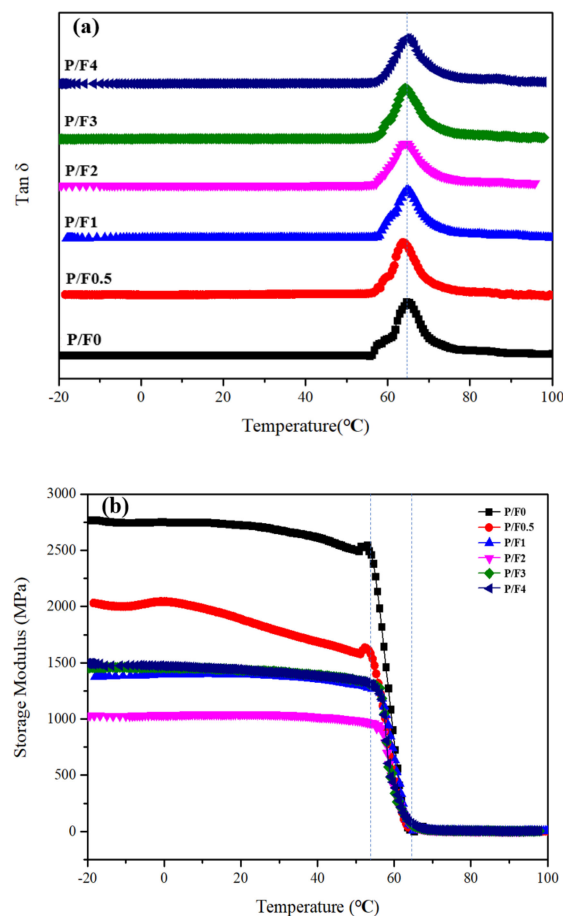
Figure 11. P/F film of (**a**) tan δ (**b**) storage modulus change diagram.

4. Conclusions

In this paper, P/F films were prepared, and the effects of different amounts of CeF_3 on mechanical properties, visible light transmittance, thermal stability and crystallinity were studied. The results are as follows: The tensile strength and elongation at break of the P/F films increased first and then decreased with the increase in CeF_3 content. The tensile strength of P/F1 was 59.92 MPa and the elongation at break of P/F2 was 2.53%, which was 8.76% and 78% higher than that of pure PLA, respectively. UV-vis transmittance analysis showed that CeF_3 had little effect on the transparency of P/F films. When the content of CeF_3 in PLA was 1 wt %, the visible light transmittance retention ratio of the P/F0 film was 82.36%. DSC analysis showed that CeF_3 promoted the crystallization of PLA; compared to pure PLA, the crystallinity of P/F1 increased by 56%. TG analysis showed that the initial degradation temperature of the P/F2 films was 330.8 °C, and the maximum degradation temperature was 364.2 °C, which was 15.1 and 10.1 °C higher than that of pure PLA, respectively. DMA analysis showed that the addition of CeF_3 could reduce the storage modulus of P/F effectively; the storage modulus (E′) of the P/F2 films was 1000 MPa, which was 63.6% lower than that of pure PLA, indicating that CeF_3 had a toughening effect on the PLA film. As a result, CeF_3 can improve the performance of PLA without affecting transparency, which had a potential application value in the field of food packaging.

Author Contributions: Conceptualization, Y.W. and F.L.; methodology, Y.W., C.Z. and J.L.; validation, S.W., X.H. and J.L.; formal analysis, Y.W. and F.L.; investigation, Y.W. and X.L.; resources, X.H., Y.L. and L.S.; data curation, Y.W., C.Z. and X.L.; writing—original draft preparation, Y.W. and J.L.; writing—review and editing, L.S., T.D. and Y.L.; visualization, Y.W.; supervision, L.S. and Y.L.; project administration, T.D. and J.L.; funding acquisition, Y.L. and L.S. All authors have read and agreed to the published version of the manuscript.

Conflicts of Interest: The authors declare no conflict of interest.

References

1. Nilsen-Nygaard, J.; Fernandez, E.; Radusin, T.; Rotabakk, B.; Sarfraz, J.; Sharmin, N.; Sivertsvik, M.; Sone, I.; Pettersen, M.K. Current status of biobased and biodegradable food packaging materials: Impact on food quality and effect of innovative processing technologies. *Compr. Rev. Food Sci. Food Saf.* **2021**, *20*, 1333–1380. [CrossRef]
2. Rai, P.; Mehrotra, S.; Priya, S.; Gnansounou, E.; Sharma, S. Recent advances in the sustainable design and applications of biodegradable polymers. *Bioresour. Technol.* **2021**, *325*, 124739. [CrossRef]
3. Din, M.; Ghaffar, T.; Najeeb, J.; Hussain, Z.; Khalid, R.; Zahid, H. Potential perspectives of biodegradable plastics for food packaging application-review of properties and recent developments. *Food Addit. Contam. Part A* **2020**, *37*, 665–680. [CrossRef] [PubMed]
4. Reichert, C.; Bugnicourt, E.; Coltelli, M.; Cinelli, P.; Lazzeri, A.; Canesi, I.; Braca, F.; Martinez, B.; Alonso, R.; Agostinis, L.; et al. Bio-based packaging: Materials, modifications, industrial applications and sustainability. *Polymers* **2020**, *12*, 1558. [CrossRef] [PubMed]
5. Wang, G.; Zhang, D.; Wan, G.; Li, B.; Zhao, G. Glass fiber reinforced PLA composite with enhanced mechanical properties, thermal behavior, and foaming ability. *Polymer* **2019**, *181*, 121803. [CrossRef]
6. Kotiba, H.; Mosab, K.; Muhammad, A.; Jinho, J.; Fawaz, D. Polylactic acid blends: The future of green, light and tough. *Prog. Polym. Sci.* **2018**, *85*, 83–127.
7. Manral, A.; Ahmad, F.; Chaudhary, V. Static and dynamic mechanical properties of PLA bio-composite with hybrid reinforcement of flax and jute. *Mater. Today Proc.* **2019**, *25*, 577–580. [CrossRef]
8. Zhu, L.; Qiu, J.; Liu, W.; Sakai, E. Mechanical and thermal properties of rice Straw/PLA modified by nano Attapulgite/PLA interfacial layer. *Compos. Commun.* **2019**, *13*, 18–21. [CrossRef]
9. Shoaib, M.; Zubair, A.; Farid, T.; Jolly, B.; Shakoor, R.; Al-Thani, N.J. PLA-TiO$_2$ nanocomposites: Thermal, morphological, structural, and humidity sensing properties. *Ceram. Int.* **2018**, *44*, 16507–16513.
10. Singla, R.; Zafar, M.; Maiti, S.; Ghosh, A. Physical blends of PLA with high vinyl acetate containing EVA and their rheological, thermo-mechanical and morphological responses. *Polym.Test.* **2017**, *63*, 398–406. [CrossRef]
11. Maria, L.; Roxanne, O.; Mario, M.; Paolo, R.; Yves, G. Peculiar crystallization kinetics of biodegradable poly(lactic acid)/poly(propylene carbonate) blends. *Polym. Eng. Sci.* **2015**, *55*, 2698–2705.
12. Xiong, Z.; Dai, X.; Na, H.; Tang, Z.; Zhang, R.; Zhu, J. A toughened PLA/Nanosilica composite obtained in the presence of epoxidized soybean oil. *J. Appl. Polym. Sci.* **2015**, *132*, 41220. [CrossRef]
13. Scaffaro, R.; Sutera, F.; Mistretta, M.; Botta, L.; Mantia, F. Structure-properties relationships in melt reprocessed PLA/hydrotalcites nanocomposites. *Express Polym. Lett.* **2017**, *11*, 555–564. [CrossRef]
14. Scaffaro, R.; Lopresti, F.; Maio, A.; Sutera, F.; Botta, L. Development of polymeric functionally graded scaffolds: A brief review. *J. Appl. Biomater. Funct. Mater.* **2016**, *15*, 107–121. [CrossRef]
15. Farah, S.; Anderson, D.; Langer, R. Physical and mechanical properties of PLA, and their functions in widespread applications—A comprehensive review. *Adv. Drug Deliv. Rev.* **2016**, *107*, 367–392. [CrossRef] [PubMed]
16. Singhvi, M.; Zinjarde, S.; Gokhale, D. Polylactic acid: Synthesis and biomedical applications. *J. Appl. Microbiol.* **2019**, *127*, 1612–1626. [CrossRef] [PubMed]
17. Zhao, X.; Hu, H.; Wang, X.; Yu, X.; Zhou, W.; Peng, S. Super tough poly(lactic acid) blends: A comprehensive review. *RSC Adv.* **2020**, *10*, 13316–13368. [CrossRef]
18. Sinclair, R. The case for polylactic acid as a commodity packaging plastic. *J. Macromol. Sci. Part A* **1996**, *33*, 585–597. [CrossRef]
19. Garlotta, D. A literature review of poly(lactic acid). *J. Polym. Environ.* **2001**, *9*, 63–84. [CrossRef]
20. Bhuvanesh, G.; Nilesh, R.; Jöns, H. Poly(lactic acid) fiber: An overview. *Prog. Polym. Sci.* **2007**, *32*, 455–482.
21. Castro-Aguirre, E.; Iñiguez-Franco, F.; Samsudin, H.; Fang, X.; Auras, R. Poly(lactic acid)—Mass production, processing, industrial applications, and end of life. *Adv. Drug Deliv. Rev.* **2016**, *107*, 333–366. [CrossRef]
22. Jem, K.; Tan, B. The development and challenges of poly (lactic acid) and poly (glycolic acid). *Adv. Ind. Eng. Polym. Res.* **2020**, *3*, 60–70. [CrossRef]
23. Mangaraj, S.; Yadav, A.; Bal, L.; Dash, S.; Mahanti, N. Application of biodegradable polymers in food packaging industry: A comprehensive review. *J. Packag. Technol. Res.* **2018**, *3*, 77–96. [CrossRef]
24. Karkhanis, S.; Matuana, L. Extrusion blown films of poly(lactic acid) chain-extended with food grade multifunctional epoxies. *Polym. Eng. Sci.* **2019**, *59*, 2211–2219. [CrossRef]
25. Zhu, X.; Yong, Y.; Feng, J.; Zhang, X.; Zhang, C.; Tang, Z.; Jin, Z. Preparation and characterization of poly(lactic acid)/starch composites toughened with epoxidized soybean oil. *Carbohyd. Polym.* **2013**, *92*, 810–816.
26. Saeidlou, S.; Huneault, M.; Li, H.; Park, C. Poly(lactic acid) crystallization. *Prog. Polym. Sci.* **2012**, *37*, 1657–1677. [CrossRef]
27. Zhang, X. Effect of poly(lactic acid) crystallization on its mechanical and heat resistance performances. *Polymer* **2020**, *212*, 123280.
28. Rubino, L. Processing technologies for poly(lactic acid). *Prog. Polym. Sci.* **2008**, *33*, 820–852.

29. Zhen, W.; Zheng, Y. Synthesis, characterization, and thermal stability of poly (lactic acid)/zinc oxide pillared organic saponite nanocomposites via ring-opening polymerization of d, l-lactide. *Polym. Advan. Technol.* **2016**, *27*, 606–614. [CrossRef]

30. Jiang, L.; Shen, T.; Xu, P.; Zhao, X.; Li, X.; Dong, W.; Ma, P.; Chen, M. Crystallization modification of poly(lactide) by using nucleating agents and stereocomplexation. *E-Polymers* **2015**, *16*, 1–13. [CrossRef]

31. Pilić, B.; Radusin, T.; Ristić, I.; Clara, S.; Lazić, V.; Baloš, S.; Donatella, D. Hydrophobic silica nanoparticles as reinforcing filler for poly (lactic acid) polymer matrix. *Hem. Ind.* **2016**, *70*, 15. [CrossRef]

32. Ivan, S.; Tanja, R.; Branka, P.; Suzana, C.; Jaroslava, B. The influence of isosorbide on thermal properties of poly(L-lactide) synthesized by different methods. *Polym. Eng. Sci.* **2013**, *53*, 1374–1382.

33. Harris, A.; Lee, E. Improving mechanical performance of injection molded PLA by controlling crystallinity. *J. Appl. Polym. Sci.* **2010**, *107*, 2246–2255. [CrossRef]

34. Nam, J.; Ray, S.; Okamoto, M. Crystallization behavior and morphology of biodegradable polylactide/layered silicate nanocomposite. *Macromolecules* **2003**, *36*, 7126–7131. [CrossRef]

35. Bai, H.; Huang, C.; Xiu, H.; Zhang, Q.; Fu, Q. Enhancing mechanical performance of polylactide by tailoring crystal morphology and lamellae orientation with the aid of nucleating agent. *Polymer* **2014**, *55*, 6924–6934. [CrossRef]

36. Wang, L.; Wang, Y.; Huang, Z.; Weng, Y. Heat resistance, crystallization behavior, and mechanical properties of polylactide/nucleating agent composites. *Mater. Des.* **2015**, *66*, 7–15. [CrossRef]

37. Bai, H.; Zhang, W.; Deng, H.; Zhang, Q.; Fu, Q. Control of crystal morphology in poly(L-lactide) by adding nucleating agent. *Macromolecules* **2011**, *44*, 1233–1237. [CrossRef]

38. Fan, Y.; Zhu, J.; Yan, S.; Chen, X.; Yin, J. Nucleating effect and crystal morphology controlling based on binary phase behavior between organic nucleating agent and poly(l-lactic acid). *Polymer* **2015**, *67*, 63–71. [CrossRef]

39. Mondal, K.; Sakurai, S.; Okahisa, Y.; Goud, V.; Katiyar, V. Effect of cellulose nanocrystals derived from dunaliella tertiolecta marine green algae residue on crystallization behaviour of poly(lactic acid). *Carbohydr. Polym.* **2021**, *261*, 117881. [CrossRef]

40. Kolstad, J. Crystallization kinetics of poly(L-Lactide-Co-Meso-Lactide). *J. Appl. Polym. Sci.* **2015**, *62*, 1079–1091. [CrossRef]

41. Li, H.; Huneault, M. Effect of nucleation and plasticization on the crystallization of poly(lactic acid). *Polymer* **2007**, *48*, 6855–6866. [CrossRef]

42. Yu, F.; Tao, L.; Zhao, X.; Yu, X.; Ai, L.; Wang, J. Effects of talc on the mechanical and thermal properties of polylactide. *J. Appl. Polym. Sci.* **2012**, *125*, E99–E109. [CrossRef]

43. Ogata, N.; Jimenez, G.; Kawai, H.; Ogihara, T. Structure and thermal/mechanical properties of poly(l-lactide)-clay blend. *J. Polym. Sci. Pol. Phys.* **2015**, *35*, 389–396. [CrossRef]

44. Chetan, S.; Mukul, S. Mechanical, optical and antibacterial properties of polylactic acid/polyethylene glycol films reinforced with MgO nanoparticles-ScienceDirect. *Mater. Today Proc.* **2018**, *5*, 20711–20718.

45. Islam, M.; Islam, M.; Islam, K. The effect of $CaCO_3$ nanoparticles and chitosan on the properties of PLA based biomaterials for biomedical applications-ScienceDirect. *Encycl. Renew. Sustain. Mater.* **2020**, *2*, 736–745.

46. Roulhac, P.; Palenik, G. Bond valence sums in coordination chemistry. The calculation of the oxidation state of cerium in complexes containing cerium bonded only to oxygen. *Inorg. Chem.* **2003**, *42*, 118–121. [CrossRef]

47. Jzab, C.; Hp, A.; Hy, A.; Jb, A.; Hza, D.; Ge, G.; Ld, A. Study on miscibility, thermal properties, degradation behaviors, and toughening mechanism of poly(lactic acid)/poly (ethylene-butylacrylate-glycidyl methacrylate) blends. *Int. J. Biol. Macromol.* **2020**, *143*, 443–452.

48. Su, Z.; Li, Q.; Liu, Y.; Hu, G.; Wu, C. Compatibility and phase structure of binary blends of poly(lactic acid) and glycidyl methacrylate grafted poly(ethylene octane). *Eur. Polym. J.* **2009**, *45*, 2428–2433. [CrossRef]

49. Zaccaria, C.; Cedrati, V.; Nitti, A.; Chiesa, E.; Pasini, D. Biocompatible graft copolymers from bacterial poly(-glutamic acid) and poly(lactic acid). *Polym. Chem.* **2021**, *26*, 3784–3793. [CrossRef]

50. Jia, S.; Chen, Y.; Yu, Y.; Han, L.; Zhang, H.; Dong, L. Effect of ethylene/butyl methacrylate/glycidyl methacrylate terpolymer on toughness and biodegradation of poly (l-lactic acid). *Int. J. Biol. Macromol.* **2019**, *127*, 415–424. [CrossRef]

51. Terzopoulou, Z.; Klonos, P.; Kyritsis, A.; Tziolas, A.; Avgeropoulos, A.; Papageorgiou, G.; Bikiaris, D. Interfacial interactions, crystallization and molecular mobility in nanocomposites of Poly(lactic acid) filled with new hybrid inclusions based on graphene oxide and silica nanoparticles. *Polymer* **2019**, *166*, 1–12. [CrossRef]